Spray Imaging and Droplet Sizing of Spark-Eroded and Laser-Drilled Injectors with Gasoline-Butanol and Gasoline-Ethanol Blends

P.G. Aleiferis and M.K. Behringer
Department of Mechanical Engineering, University College London, UK

D. OudeNijeweme and P. Freeland
MAHLE Powertrain, UK

ABSTRACT

The spray atomisation characteristics of gasoline, ethanol, butanol and blends of gasoline with 16% butanol, 25% butanol and 25% ethanol were investigated for two 7-hole injectors by optical diagnostics. One of the injectors had its nozzle holes drilled by common spark erosion whilst the other one was its 'direct replacement' that had its holes formed by Laser drilling. The nozzle holes were initially analysed to understand the differences in their geometry. Then high-speed spray imaging was performed in a quiescent injection chamber by Laser illumination. The spray images were statistically analysed over a series of injection events per test condition to obtain spray tip penetration and velocity, as well as various spray angles. Furthermore, droplet sizing was conducted by Phase Doppler Anemometry (PDA). A single spray plume was isolated for this and measurements were obtained across the plume at a distance of 25 mm downstream of the nozzle exit. All tests were performed with 120 bar fuel pressure at two gas pressures, 0.5 bar and 1.0 bar, and two injector temperatures, 20 °C and 80 °C, to examine effects relevant to typical cold and warm engine conditions with early intake injection strategies.

1. INTRODUCTION

1.1 Background

The design of new direct injection systems for spark-ignition engines is very important for optimised mixture formation strategies with different fuels and low exhaust emissions, including particulates that are central to EU6 regulations. It is preferable to meet the proposed targets by means of engine internal measures rather than separate treatment in the exhaust system that can be associated with a CO_2 penalty. Latest injector manufacturing methods by Laser-drilling have shown some promising results. Specifically, Whitaker *et al.* [1] showed a significant reduction in particulates using a Laser-drilled in comparison to a spark-eroded multi-hole injector; however, in their study the exact nozzle design was not specified. As particulates are generally attributed to poor atomisation, wall wetting and incomplete air-fuel mixing, it is important to understand the differences in fuel spay formation between spark-eroded and Laser-drilled injectors. The challenge is further complicated by the predicted fuel stock that may contain significant amounts of biofuels. Ethanol is to date still one of the preferred renewable additives or substitutes to gasoline. Amongst its favourable properties is the fuel Research

Octane Number (RON) enhancing capability; its high latent heat of evaporation can also be exploited in parallel to its high RON and enable even higher compression ratios due to charge cooling effects. The addition of 10% ethanol to gasoline (E10) is the legal maximum (legislation is based on oxygen content) in the USA for use with standard vehicles, while flex-fuel vehicles need to be used for higher ethanol contents. E10 is also already commonplace in Europe. Butanol is also believed to be a new alternative fuel with potential to play a strong role. Current ethanol production plants can be updated to produce butanol and the use of butanol may not require major modifications to the current infrastructure of gasoline transportation and use as it is also more compatible with most typical materials already used in these processes, including injection system technologies; this is in contrast to ethanol's not direct compatibility. Butanol is also less hygroscopic than ethanol, has lower vapour pressure and its heating value is higher than ethanol's. Butanol production processes are already established and have the potential to be widened to have similar capabilities to ethanol production. Special interest exists for blends of gasoline with 16% butanol (B16). B16 is similar to E10 in terms of oxygen content. Furthermore, low percentages of butanol feature distillation curves similar to conventional gasoline. Ethanol mixtures exceeding 10% in gasoline have been considered problematic as ethanol tends to concentrate in the low-carbon fractions of gasoline and shifts the distillation curve to higher volatility at lower temperatures. This is an undesirable effect as volatility limits need to be controlled for legislative reasons. Low butanol blends do not show the same behaviour. The combined effects of vapour pressure, viscosity, surface tension, *etc.*, with variation of ethanol and butanol content in gasoline, although of great importance for spray formation and mixture preparation in engines, are not well understood. However, legalisation of higher percentage ethanol blends in gasoline (*e.g.* E15) is being discussed in US by the Environmental Protection Agency. Such legalisation would, based on oxygen content, also open the door for legalisation of up to B25 blends. Similar percentages of ethanol in gasoline, *e.g.* E25, may then also be considered as a long term possibility, especially if research shows viability.

1.2 Present contribution

The process of Laser drilling injector holes can allow flexibility in the manufacturing implementation of specific nozzle geometries to control the features of in-nozzle flow and cavitation. There are no major publications that have compared the atomisation characteristics from spark-eroded and Laser-drilled injectors, especially in the context of various types of fuel blends for spark-ignition engines. The work described in this paper was aimed at understanding the mechanism of spray formation from two injectors for direct-injection spark-ignition engines, one spark-eroded and its 'like-for-like' replacement Laser-drilled injector. The main objectives of the study can be summarized as follows:

- Study the effect of fuel type on spray formation with both injectors using gasoline, ethanol, E25, butanol, B16 and B25.
- Analysis of the spray's development characteristics using high-speed imaging.
- Quantification of the spray's features, namely penetration during the injection event and outer spray envelope cone angles.
- Droplet sizing by Phase Doppler Anemometry (PDA).
- Obtain fuel properties for longer term analysis of the spray data.

2. FUELS

2.1 Fuels tested and their properties

The gasoline-alcohol mixtures B16, B25 and E25 were benchmarked against the individual base components ethanol and *n*-butanol. The gasoline used was pump-grade RON95. *Iso*-octane and *iso*-octane-alcohol blends (B16I84, B25I75 and E25I75) were also included in parts of the study (although results have not been

explicitly included in the current paper), as *iso*-octane is a single component reference fuel typically used in engine research with well-known thermophysical properties, hence relevant data can be useful in the community for comparison with previous work on other injectors. All the single components were of chemical grade purity and all mixtures were splash-blended on a volumetric basis. **Table 1** and **Table 2** give an overview of fuel properties relevant to atomisation. Properties of single components at 20 °C and 80 °C were obtained from [2]. If not specified differently, data for gasoline were taken from product data sheets. The densities at 20 °C were measured for all fuels as mass per volume. Viscosities, surface tension, vapour pressures and distillation curves were measured as discussed in the next two sections. Chen and Stone [3] measured the enthalpies of vaporisation of *iso*-octane-ethanol blends as proxy for gasoline-ethanol blends and found a linear relationship with volumetric mixture percentage. No such information could be found in the literature for butanol-gasoline or butanol-*iso*-octane blends but a similar trend as for ethanol's blends was assumed. The values for specific heat and latent heat (relevant to Jacob number effects) were linearly interpolated according to mass percentages of the pure components. Mass weighting was also used for density estimates at 80 °C that could not be established due to bubbling.

Table 1. Properties of basic fuels.

Fuel	Ethanol	Butanol	Gasoline	*iso*-Octane
Chemical formula	C_2H_5OH	C_4H_9OH	$\sim C_4–C_{12}$	C_8H_{18}
Molar mass [g/mol]	46.07	74.12	100–105	114.3
Density, 20 °C, 80 °C [g/cm^3]	0.79, 0.73	0.81, 0.76	0.72, 0.66	0.69, 0.64
Solubility in water (20 °C) [g/l]	miscible	79	partially	immiscible
DVPE, 20 °C [kPa]	6.4	0.8	35	5.7
DVPE, 37.8 °C (~RVP) [kPa]	16.1	2.2	72.4	11.8
DVPE, 80 °C [kPa]	100	16.4	208	50
Kinematic viscosity, 23 °C [cSt]	1.33	3.22	0.47	0.62
Kinematic viscosity, 80 °C [cSt]	0.60	0.99	0.25	0.40
Surface tension, 23 °C [mN/m]	23.01	25.50	21.80	18.78
Surface tension, 80 °C [mN/m]	16.4	19.3	–	13.6
Latent heat, 25 °C [kJ/kg]	874	669	380–500	300
Latent heat (at boiling) [kJ/kg]	855	584	364	272
Specific heat, c_p, 25 °C [kJ/kgK]	2.46	2.30	2.22	2.09

Table 2. Properties of blends.

Fuel	E25	E25I75	B16	B25	B16I84	B25I75
Molar mass [g/mol]	78	81	96	93	104	99
Density, 20 °C [g/cm^3]	0.76	0.71	0.75	0.75	0.70	0.72
Density, 80 °C [g/cm^3]	0.68	0.66	0.70	0.70	0.65	0.67
DVPE, 20 °C [kPa]	38	11	32	30	8	8
DVPE, 37.8 °C (~RVP) [kPa]	73.8	26.5	66.3	62.9	14.7	14.4
DVPE, 80 °C [kPa]	240	140	194	188	70	69
Kinematic viscosity, 20 °C [cSt]	0.75	0.89	0.68	0.79	0.83	1.00
Kinematic viscosity, 80 °C [cSt]	0.37	0.58	0.34	0.39	0.54	0.55
Surface tension, 23 °C[mN/m]	21.5	19.3	21.0	21.5	18.7	18.8
Latent heat, 25 °C [kJ/kg]	491	433	401	422	329	360
Specific heat, c_p, 25 °C [kJ/kgK]	2.28	2.18	2.23	2.28	2.12	2.14

2.2 Measurement of distillation curves and vapour pressures

Vapour pressures and distillation curves were measured following ISO 17025, with distillation according to ASTM D86 and vapour pressure according to IP394 to obtain ASVP (air saturated vapour pressure) and DVPE (dry vapour pressure equivalent), the latter by a statistical correlation to Reid vapour pressure (RVP). The most obvious feature of the distillation curves in **Figure 1** is that E25, B16 and B25 all start below gasoline but, while the butanol mixtures exceed the recovered

volume of gasoline at ~105 °C and ~110 °C respectively, the ethanol mixture surpassed gasoline at ~55 °C. **Figure 1** also shows that E25's vapour pressure exceeds significantly that of both base fuels. Butanol did not show this behaviour; the vapour pressures of B16 and B25 were very close to each other and both laid below gasoline's and above pure butanol's. However, as shown in **Table 2**, when ethanol or butanol was mixed with *iso*-octane, the resulting vapour pressures were in both cases above their base components; nevertheless, E25's vapour pressure was much higher than B25's. Distillation curves of gasoline blends with ethanol or butanol in [4] have also illustrated that low percentage mixtures of ethanol increased the RVP above that of the base fuels, whilst butanol addition to gasoline resulted in RVP between gasoline's and butanol's. The RVP of the alcohol-gasoline blends of [5] were slightly lower than those measured here; differences can be linked to the specifics of the base gasoline fuel. Similar RVP reduction was found in the present work for the butanol-*iso*-octane mixtures. The RVP of E25I75 showed good agreement with interpolated data at 35 °C from [6] and at 60 °C from [7].

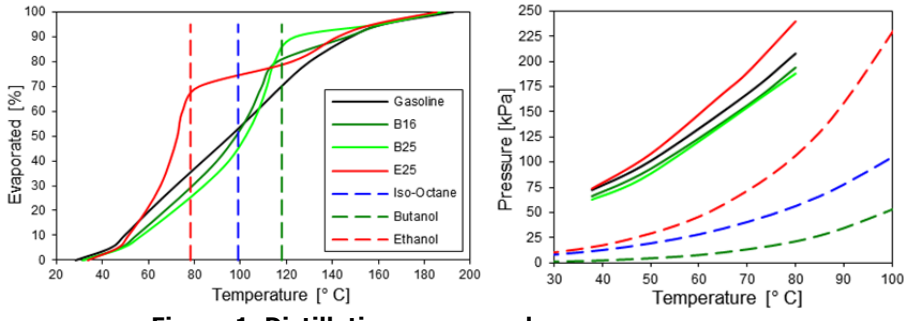

Figure 1. Distillation curves and vapour pressures.

2.3 Measurement of kinematic viscosity and surface tension

Measurements of kinematic viscosity were obtained for all fuels using a Brookfield LV DVIII Ultra SC4-18 viscometer. The results have been included in **Tables 1–2**. At 80 °C, some of the fuels could not be measured due to onset of bubbling; gasoline, B16, B25 and E25 were affected. The values shown were instead based on the reduction seen for the respective blends with *iso*-octane as these were measured without any issues of bubbling. While such an approach may lead to good estimates for high-pressure conditions inside the injector body, the complex multi-phase phenomena when the fuel is released through the nozzle into the combustion chamber may lead to deviations. Mixing butanol with gasoline increased the kinematic viscosity, however, the value was far below pure butanol's. Ethanol's viscosity was also high at cold conditions; mixing it with gasoline or *iso*-octane improved the situation. The mixtures had a viscosity that was ~40–70% higher than gasoline's. Values of surface tension were measured using a KRÜSS drop shape analysis DSA100 system. The system did not provide an option for measurements at elevated fuel temperatures. **Table 1** and **Table 2** include all the measured surface tension values. The values of ethanol and butanol were higher than gasoline's and much higher than *iso*-octane's. The mixtures showed values very close to *iso*-octane's, even lower than gasoline's. For the single components, values at 80 °C were acquired from [2] and then estimates were obtained for *iso*-octane's blends with the alcohols using percentage weighting.

3. INJECTORS

3.1 Geometry of nozzles

Two 7-hole injectors designed for side mounting in engine combustion chambers were the focus of this investigation. The first injector had a standard spark-eroded

(SE) nozzle while the second was the manufacturer's 'direct replacement', made using Laser drilling (LD) technology. The manufacturing process of Laser drilling can allow implementation of complex geometrical aids to promote or suppress turbulence and cavitation. The overall nozzle tip layout is shown in **Figure 2(a)**. Despite being direct replacements, initial visual inspection under a microscope revealed a similar stepped hole pattern but different diameters; hence, silicone castings were then obtained according to [8] to quantify details of the inner hole and surface quality. The results are shown in **Figure 2(b)** where the large vertical arrows indicate flow direction.

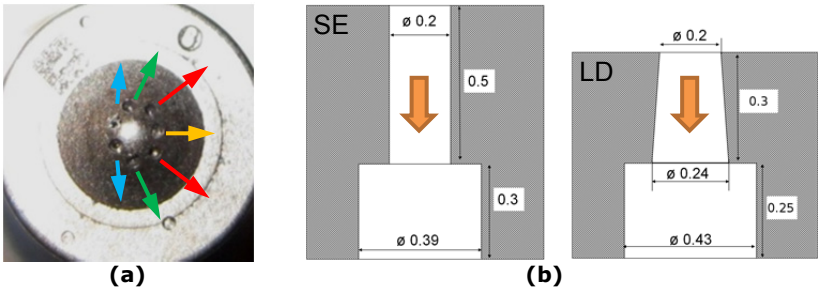

(a) **(b)**

Figure 2. (a) 7-hole injector pattern, (b) nozzle-hole geometries.

It was found that the SE injector featured an inner spark-eroded cylindrical bore with a diameter of 0.2 mm and a length of ~0.5 mm, before opening up into a hole with a diameter of 0.39 mm and a depth of ~0.3 mm. This step is commonly associated with benefits regarding reduction of nozzle deposits. The injector-hole design features regions of flow separation. At the entrance of the inner bore a *vena contracta* is formed that reduces the effective diameter (by a factor of ~0.6). A re-circulation area is hence formed at the inlet edge, leading to low local pressure and increased turbulence, hence promoting the onset of cavitation. When the flow enters the larger outer hole, similar phenomena are expected, coupled to immediate primary breakup. The outer hole of the second injector remained conventionally drilled by spark erosion and was cylindrical with a diameter of ~0.43 mm and a length of ~0.3 mm. The inner nozzle was manufactured by Laser drilling and the hole was of conical shape with a start diameter of ~0.2 mm, opening up to ~0.24 mm over a distance of ~0.3 mm. Such differences highlighted immediately the necessity for flow and spray analysis. For example, the increased surface smoothness of Laser drilling (observed under an electron microscope) reduces the friction factor, in addition to different losses originating from the shorter conically shaped nozzle. The LD's conical hole created a more acute angle at the entrance (by ~4°) and the incoming liquid fuel would experience a stronger flow separation. The separation region could also be maintained for longer due to the increasing hole diameter. This could induce cavitation more readily. The opposing effect in converging nozzles (tapered) is already used to suppress cavitation in high-pressure Diesel injectors where cavitation may have destructive effects. Regarding turbulence, the effect of the conical hole is not immediately clear, especially in the presence of cavitation. As the entry into the flow channel was of the same size for both injectors, the respective Reynolds, Weber and Ohnesorge numbers would be same for same flow rates between injectors. However, with different losses past that entry and differences in the effective hole diameter from phase change effects, the Reynolds numbers would be different as the discharge coefficients would be different. In contrast, the conical nozzle would lead to flow relaxation but the short length and flow momentum might not allow flow adaption as the residence time in the nozzle would be very short and the difference in inferred turbulence may not be as large as expected if the outer hole diameter was used for Reynolds estimation. Furthermore, initial droplet sizes are often based on the nozzle diameter (or at least of the same order). However, the actual diameter may be of reduced significance in

the presence of strong cavitation where the process of exiting is accompanied by violent liquid disruption. In the absence of cavitation, fuels with low vapour pressure and high viscosity, like butanol, would be greatly affected.

3.2 Flow rate measurements

To establish flow rates and calculate nozzle flow velocities and associated Reynolds, Weber and Ohnesorge numbers, fuel injection quantities were measured for gasoline, ethanol and butanol with both injectors. The injector pulse length was varied for gasoline whilst the other fuels were compared at fixed injection duration of 1.26 ms. Measurements were taken with 80 bar and 120 bar fuel pressure, at 1.0 bar ambient pressure, for 20 °C and 80 °C injector body temperature. Both injectors featured an injection delay of ~0.25 ms. The measured flow rate of the LD injector was ~10% above that of the SE. This was initially surprising considering that these were 'like-for-like' replacements and matched flow rates were presumed. The larger flow rate of the LD was most probably by design as shorter injection durations would be required at fixed load, more time would be allowed for mixing and/or spray wall impingement could be reduced. **Figure 3** shows the injected quantities of both injectors with 1.26 ms pulse duration. Higher temperatures increased butanol's flow rate through the SE injector, while all other fuels showed a decrease in injected quantities. The decrease was strongest for gasoline. Cavitation and flash boiling effects can be the main cause for such reduction, as the lower fuel viscosity on its own should have increased the flow rate at higher temperature. The latter was probably dominant for butanol though, whose flow rate increased.

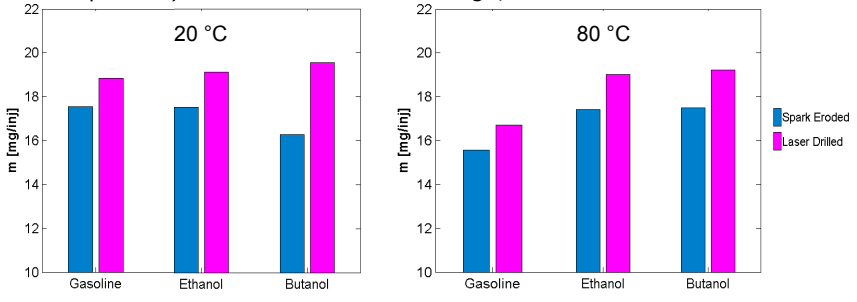

Figure 3. Injected fuel quantities (120 bar fuel pressure, 1.0 bar air).

4. EXPERIMENTAL SETUP AND DIAGNOSTICS

4.1 Injection chamber

A cylindrical quiescent injection chamber was used for the current work, as shown in **Figure 4**. Its inside diameter was 180 mm and its height 300 mm. The top cover was protruding into the chamber giving a final volume of ~7 l. The side walls had cut-outs for four circular windows with an inside diameter of 95 mm, spaced 90° to each other. The fused silica windows were 32 mm thick, had a transmittance of 93% (@ 355 nm and 532 nm) and were optically polished to λ/10 (@ 630 nm). The injectors were placed in specially designed mounts which could be set inside the chamber's top cover. A jacket heater was placed around the injector housing so that the arrangement could be controlled up to 130 °C using a Eurotherm controller and a thermocouple in the housing. The chamber was equipped with a pressure sensor (DRUCK PDCR 910), an analogue pressure gauge and a thermocouple to monitor the chamber gas pressure. A vacuum pump was connected to the chamber for sub-atmospheric pressure testing but also to purge the chamber after injections. For purging, the high pressure line was switched on using a shut-off valve controlled by a PLC module (SIEMENS LOGO! DC 12/24RC) and triggered by an AVL 427 timing unit 0.1 s after each injection event for a duration of 1.5 s. The fuel was

supplied by a Heypac pneumatic pump with regulator; a pressure transducer (OMEGA PXM4202) and an analogue pressure gauge were used to monitor the fuel pressure. The injector's driver unit was triggered by the AVL 427 timing unit.

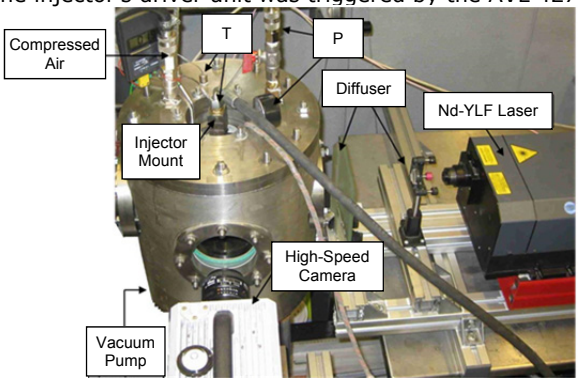

Figure 4. Injection chamber with camera and Laser arrangement.

4.2 Spray imaging

A Photron APX-RS high-speed CMOS camera was set to 9 kHz frame rate in random reset mode, taking 60 images per injection event in the chamber. This frame rate corresponded to one image per 1° crank angle (CA) for an engine operating at 1500 RPM. The injection pulse duration was set to 1.26 ms; this was equivalent to stoichiometric engine fuelling at 1500 RPM low load-operation. A Nikon Nikkor 28 mm lens and f/5.6 were selected, resulting in a depth of field of ~14 mm. The camera's internal memory allowed acquisition of 113 injection events at 640×480 pixels. The image resolution was 122 μm per pixel. A Pegasus-PIV New Wave Nd:YLF Laser at 527 nm was used for illumination. The Laser was capable of 10 kHz maximum Q-switch frequency for each of its two cavities. Only one of the cavities was employed; the beam of ~1.5 mm diameter was diffused through a lens with a very short focal distance, followed by two etched glass diffusers (to reduce speckles). Camera and incident Laser were at 90°. Images were taken mainly through one 'side' view, representative of a typical 'tumble' in-cylinder plane. For limited testing, placement of a 45° mirror inside the chamber allowed imaging of the spray's footprint too. Injection frequency was 0.2 Hz. Measurements were taken at 0.5 bar and 1.0 bar gas pressure (*i.e.* 'back' pressure) to represent low-load and full-load conditions in the intake stroke of a naturally aspirated engine. The gas temperature was monitored at ~20 °C. Fuel temperatures (injector body temperatures) of 20 °C and 80 °C were tested. Tests were performed at 80 bar and 120 bar fuel pressure but only the latter is mainly discussed here. Target of the image processing method was then to obtain spray penetration and various 'outer envelope' spray angles in accordance to the structural features proposed by [9]. In-house MATLAB-based coding was employed. The procedure consisted of thresholding and binarisation of each spray image. The methods have been published and are not repeated here for brevity [10–13]. **Figure 5** illustrates an image of the spray inside the injection chamber in side view and the processing results. Spray angles were quantified at 5 mm, 15 mm, 25 mm and 35 mm downstream of the nozzle exit. The angle formed between 5 and 15 mm past the nozzle was also quantified. The spray's penetration was determined in the axial and radial direction. The spray area and mean spray brightness was also obtained. All data were statistically

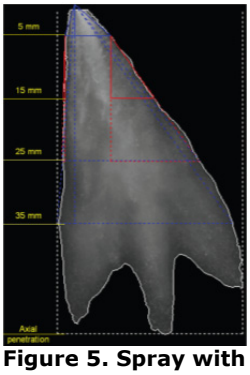

Figure 5. Spray with overlaid features.

analysed; the values presented later are averages of 113 sprays per test case. The overlaid features in **Figure 5** signify: Spray outline at intensity threshold 15 of 255; 0–5 mm angle: Near-nozzle spray angle (blue line); 0–25 mm angle: Developed spray angle (dashed blue line); 0–35 mm angle (dashed blue line); 5–15 mm angle (solid red line); axial penetration (dashed white line).

4.3 Phase Doppler Anemometry (PDA)

`Phase Doppler Anemometry (PDA) was employed for droplet sizing. The method is well established and the reader is guided to [14] for more information. The PDA system consisted of a 5W Coherent Ar^+ Laser with TSI FSA4000 signal processor and fibre probes. It was arranged for 30° off-axis forward scatter angle between transmitter and receiver as shown in **Figure 6(a)**. Three detectors were used to validate the measurements; a 25 µm slit was used in front of the receiving optics. Droplet sizing focused on a single spray plume. To do that a special micro-funnel was manufactured; this featured a curved edge which sat in touch with the injector tip. The most central plume was selected and the funnel was carefully attached to the injector tip to redirect the remaining plumes. **Figure 6(b)** illustrates the overall spray cross section and the extracted plume with the PDA measurement locations 25 mm downstream the nozzle tip. The test conditions were identical to the spray imaging test matrix; so were the injection frequency and duration. Sufficient time was included to stabilise the air-flow in the chamber after purging before the next injection. Once each test point was finished, the vacuum pump was switched off and the 1.0 bar condition was checked again before moving to the next horizontal location in intervals of 2 mm. Channel 1 (514.5 nm) was used for size and vertical velocity measurements. The photo-multiplier voltage was selected using a D10 stabilisation method and on the basis of maximum data rate. Invalid measurements from multiple occupancy, reflection instead of refraction, phase wrap and occupancy outside the $1/e^2$ beam waist were rejected. Channel 2 (488 nm) measured the horizontal droplet velocity simultaneously. The droplets were measured for 3.3 ms from the start of injection (SOI) to obtain values during the spray and after nozzle closure. The number of injections was between 100 and 400 until at least 10,000 droplets were measured at each location. Measurements in dense regions required more injections per condition due to issues of multiple occupancy and weakening of the Laser beam by obscuration and beam scatter. All data were sorted into bins of 0.111 ms (equivalent to 1° CA) for each location; both the average droplet diameter (D_{10}) and the Sauter mean diameter (SMD, D_{32}) were calculated.

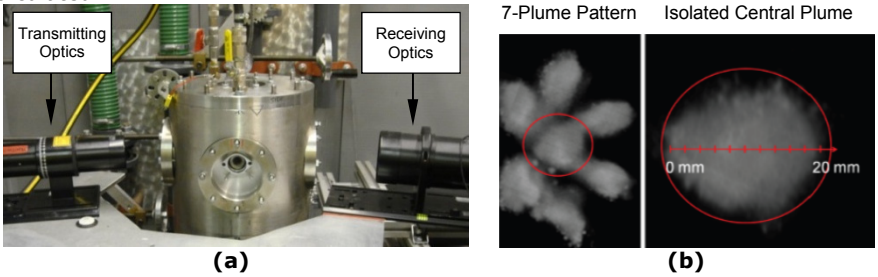

Figure 6. (a) PDA system, (b) spray with PDA locations on enlarged plume.

In addition to the fuel properties shown earlier, the refractive index was also measured for each fuel as this is an important input for PDA. An ABBE refractometer was employed. The instrument could be heated from 20 °C to 70 °C with measurements taken every 10 °C. Linear interpolation was used to extend the graphs up to 90 °C. The given refractive index was for a wavelength of 589 nm; this was corrected for the PDA's wavelength of 514 nm. The value used for PDA was for the nominal fuel temperature at injection. While it is not uncommon to use a single value for different fuels and temperatures, it was decided that it would be

better if specifically measured values were used and the effect of temperature dependence of the refractive index of the fuels was considered on the basis of previously published PDA work, *e.g.* [15, 16]. However, the correct use of the refractive index is still not without controversy and may require further work as the actual droplet temperature during injection and evaporation is neither known nor can it be considered constant over the droplet's volume, especially with different fuels of diverse thermophysical properties and over a range of conditions; see [17] for modelled droplet temperatures during evaporation.

5. RESULTS AND DISCUSSION

5.1 Visual analysis of sprays

5.1.1 Sprays of gasoline, ethanol and butanol (20 °C)

Figure 7 shows typical spray images with simultaneous side and bottom view through the 45° mirror for gasoline at 20 °C, 1.0 bar at 7° CA after start of injection (ASOI). The individual spray cones were better distinguishable for the SE injector and the images clearly indicate better spray dispersion for the LD injector. Although spray dispersion was visibly stronger for the LD injector, separate plumes were still identifiable. The bottom view also shows that the plume seen on the side view consisted of two plumes front and back, but three plumes in the centre.

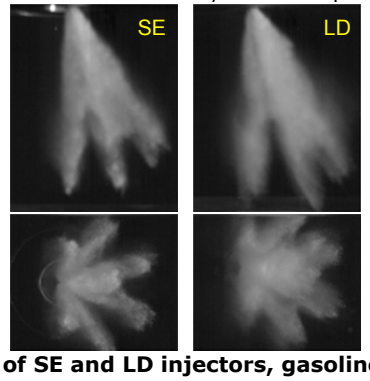

Figure 7. Sprays of SE and LD injectors, gasoline; 20 °C, 1.0 bar.

Figure 8 shows the spray development of gasoline, ethanol and butanol from 5–7° CA ASOI (0.55–0.77 ms ASOI) for typical injections at 1.0 bar gas pressure and 20 °C fuel temperature. Visual comparison of the gasoline sprays shows that the SE injector spray appeared with a slightly longer delay than that of the LD. This is linked to the larger mass flow rate of the LD injector. For all fuels shown, the LD injector featured plumes which were more dispersed and the overall spray was wider. The gasoline spray tip of the SE injector contained visibly more clusters of larger droplets than the LD. These larger droplets contained high axial momentum causing the SE injector's tip penetration to make up for the initial delay and finally overtake the spray tip of the LD injector around 8–9° CA ASOI (0.88–0.99 ms ASOI). The overall lower axial penetration of the LD injector could be beneficial due to potential for reduced piston impingement, whilst the higher radial penetration would promote mixing. For both alcohols, the first notable difference to gasoline was that the initial delay was increased with both injectors, but with the effect being stronger for the SE. Such delays with alcohol fuelling have been previously observed with other multi-hole injectors, *e.g.* [11, 13], and originate from higher fuel viscosity effects. Ethanol's spray tip droplets were visibly larger than gasoline's, especially for the SE injector. The LD injector also had a small delay in ethanol's appearance, but this was closer to gasoline's first arrival. Unlike for gasoline, the SE ethanol injection could not catch up or overtake the LD ethanol spray by 8–9° CA

ASOI. Upon close image inspection ethanol appeared again to be better dispersed with the LD injector and large tip droplets were not as prominent as with the SE. All those effects observed for ethanol can be seen for butanol, and in even more dominant form. Butanol's spray delay was increased by one additional frame (1° CA equivalent) compared to ethanol's with the SE injector, but only slightly with the LD injector. As before, the LD injector seemed to exhibit better spray dispersion and the resulting overall spray area was larger; yet the overall spray area and angle seemed to be significantly smaller for butanol compared to gasoline and ethanol.

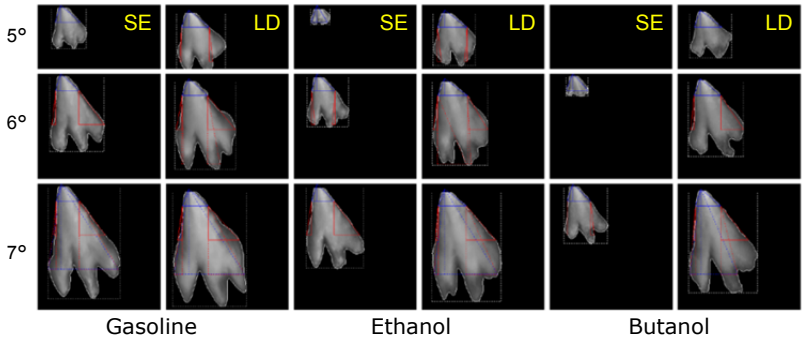

Figure 8. Spray development for SE and LD injectors; 20 °C, 1.0 bar.

5.1.2 Sprays of gasoline, ethanol and butanol (80 °C)

When the fuel temperature was increased from 20 °C to 80 °C at 1.0 bar gas pressure, the gasoline spray from both injectors showed typical signs of flash boiling and individual plumes were no longer discernible but a combined spray structure was present, propagating along the axis of the central plume, as shown in **Figure 9**. The mechanism of flash boiling and spray collapse has been described in other publications with 6-hole injectors, *e.g.* [10–13], but there the extent of collapse was less pronounced and individual plumes were still visible. The gasoline spray of the LD injector appeared again earlier than that of the SE. It maintained visibly a higher penetration throughout the imaged time window and a wider illuminated area. Ethanol, nominally just above its boiling point of 78 °C at 1.0 bar, was not flash boiling and the individual plume tips were still visible; spray collapse did not occur. At 0.5 bar, ethanol's spray shape was closer to gasoline's, even narrower and 'pointier'. As for ethanol, butanol's spray delay largely disappeared at 80 °C fuel temperature, most likely due to reduced viscosity. The spray shape was otherwise reminiscent of the 20 °C ethanol spray (which had similar viscosity at that temperature), with visibly separate plumes and clusters of large droplets at the spray tip, especially for the SE. A reduced amount of large droplets at the spray tip of the LD injector was observed for all fuels.

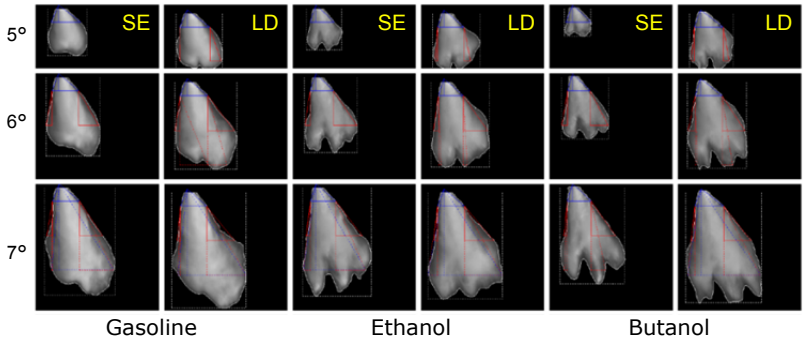

Figure 9. Spray development for SE and LD injector; 80 °C, 1.0 bar.

5.1.3 Sprays of gasoline blends with ethanol and butanol

Single typical images of the base fuels and their blends B16, B25 and E25 at 8° CA ASOI (0.88 ms ASOI) are shown in **Figure 10** for 20 °C and in **Figure 11** for 80 °C fuel temperature at both 1.0 bar and 0.5 bar gas pressure. At 20 °C, a general reduction in spray penetration with increasing alcohol content was observed for the SE injector. This could not be seen at the same extent for the LD. The mixtures were generally closer to gasoline in shape than to the pure alcohols; however, with the exception of penetration, little difference was typically distinguishable at these conditions. This changed distinctly when the temperature was raised to 80 °C. Although at 1.0 bar, gasoline showed strong collapse of the individual plumes, the gasoline-butanol mixtures retained separate plumes for the SE injector. The LD injector's sprays of B16 and B25 showed stronger merging than those of the SE but also better dispersion. E25's spray features remained similar to gasoline's with both injectors. At 80 °C, 0.5 bar, both B16 and B25 approached gasoline's spray shape with both injectors. Ethanol was fully collapsed at these conditions; even butanol's plumes started merging, showing better atomisation.

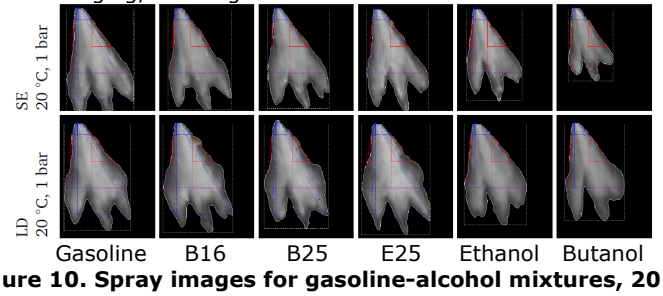

Figure 10. Spray images for gasoline-alcohol mixtures, 20 °C.

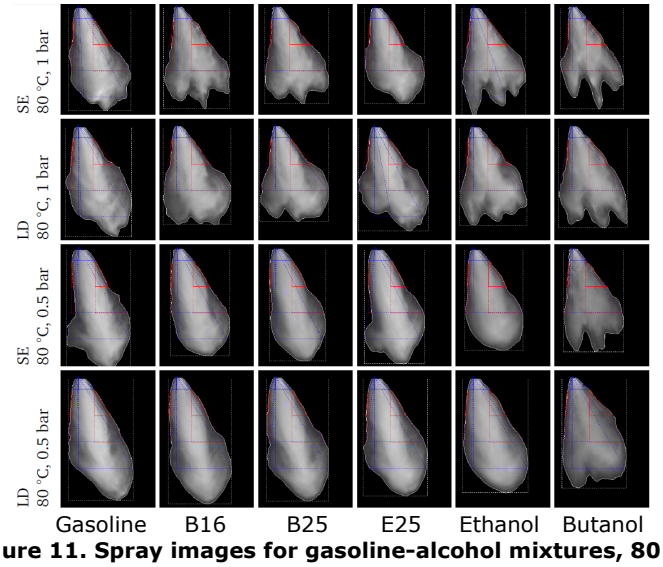

Figure 11. Spray images for gasoline-alcohol mixtures, 80 °C.

5.2 Image processing analysis of sprays

5.2.1 Spray penetration

The penetration graphs of **Figure 12** quantify the earlier visual comments for both injectors. Gasoline's initial penetration at 20 °C, 1.0 bar, for the LD injector was higher than for the SE. The spray tip velocity, calculated by the gradient of the penetration curve was initially ~100 m/s for both nozzles but quickly reduced,

almost linearly, for the LD injector. In contrast, the SE maintained a higher spray tip velocity during the initial 3–4° CA after appearance (~0.3–0.4 ms). Differences in effective aerodynamic forces for the LD injector due to its wider dispersion and/or different effects from developing in-nozzle flow and cavitation with ongoing injection may be the cause. The penetration graphs also emphasise the delay in spray appearance for the higher viscous fuels with the SE injector, by ~1° CA for ethanol, ~2° CA for butanol, and just about 0.25–0.5° CA for the mixtures, compared to gasoline.

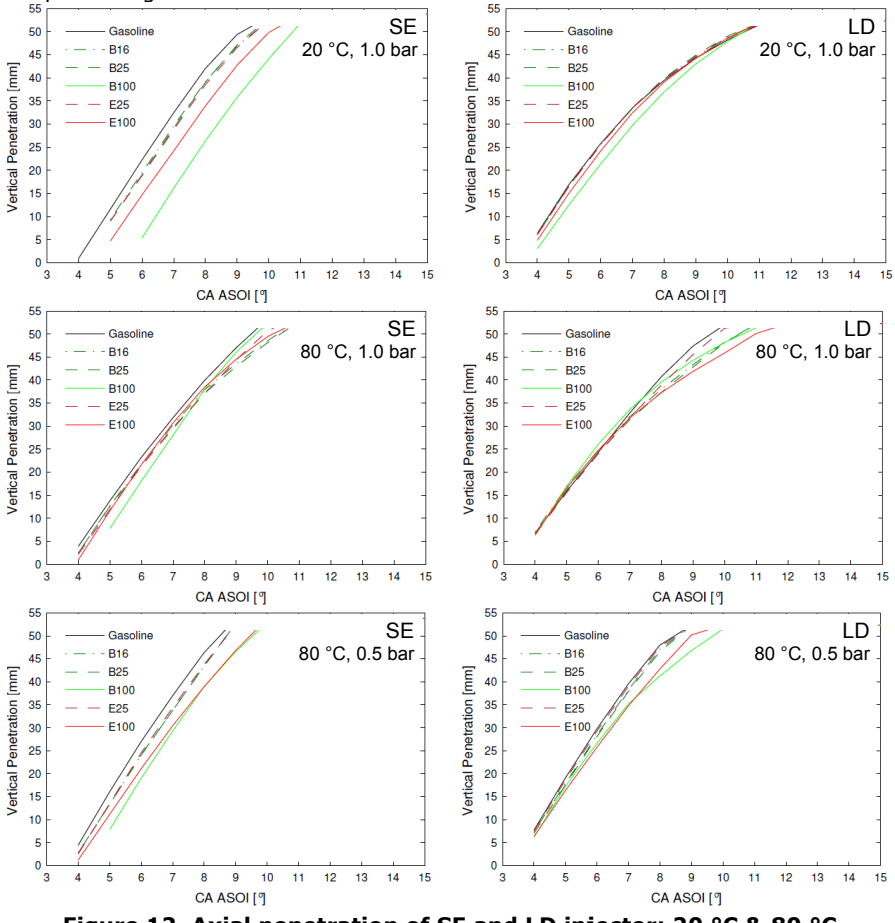

Figure 12. Axial penetration of SE and LD injector; 20 °C & 80 °C.

The differences amongst fuels were much smaller with the LD injector; only ethanol and butanol were slightly delayed by about 0.25–0.5° CA. Increasing the fuel temperature to 80 °C at 1.0 bar, the penetration and velocities of both injectors became generally more akin to each other. Initial spray tip velocities were 10–15% lower than at 20 °C. The fuels that exhibited sprays of collapsed form, *i.e.* gasoline and E25, showed larger penetrations in the later stages of injection. The SE injector was associated with faster, more linear velocity decline than at 20 °C, probably caused by the presence of smaller droplets. Butanol was not affected to the same extent like the other fuels but the reduced viscosity at 80 °C resulted in much earlier spray appearance. Similarly for the LD injector, gasoline and E25 collapsed and initially conserved their axial momentum for longer; butanol was no longer strongly delayed. The average deceleration for gasoline was ~58 mm/ms^2 for the

SE and ~76 mm/ms^2 for the LD. The collapsed spray of the flash-boiling fuels at 80 °C, 0.5 bar had higher penetration due to smaller drag and increased downwards momentum from the merged plumes. This can be critical as it can cause stronger direct piston impingement and poorer air-fuel mixing overall, potentially even worse particulate emissions, despite the smaller initial droplets from flash-boiling at these conditions. The larger penetration of the LD injector would seem disadvantaged in that respect but, if seen in the context of its higher flow rate, the injection pulse could be reduced to achieve the same injection quantity to that of the SE and counteract piston impingement effects from the stronger spray collapse. At these conditions, plume merging was visible for the butanol fuels too, with pure butanol affected the least. Spray deceleration was still stronger for the LD, with ~76 mm/ms^2 compared to ~54 mm/ms^2 for the SE. The early penetration also showed greater differences among fuels, with gasoline earlier and faster than the mixtures, followed by ethanol and butanol. The effect was clearer with the SE than the LD. The standard deviation in penetration was about 1.5 mm and in tip velocity up to 5 m/s for the SE and 3 m/s for the LD.

5.2.2 Near-nozzle spray angle (0–5 mm)

Figure 13 shows the near-nozzle 0–5 mm spray angle development. Generally, fuel appeared at 5 mm past the nozzle tip between 4–5° CA ASOI, marginally earlier for the LD injector. After an initial peak, the sprays relaxed quickly and maintained a constant angle for the duration of the injection.

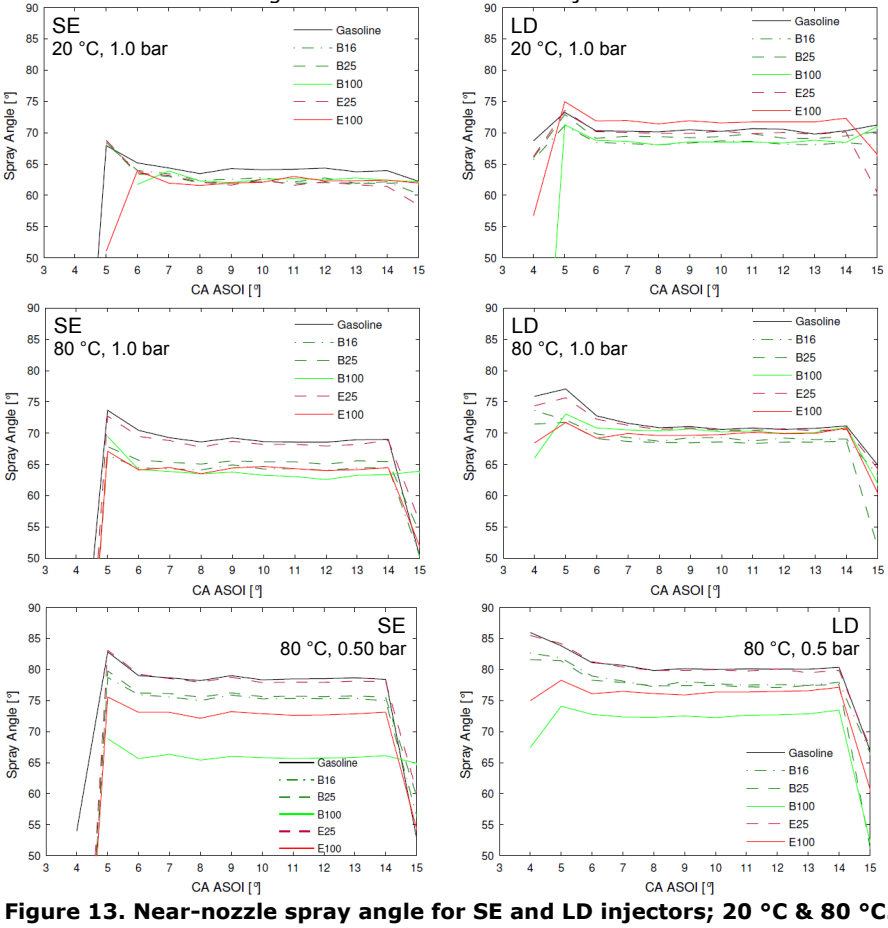

Figure 13. Near-nozzle spray angle for SE and LD injectors; 20 °C & 80 °C.

All near-nozzle angles at 20 °C, 1.0 bar were just below 65° for the SE injector with all fuels within 2° of each other. The respective angle was about 5–7° greater for the LD injector, reflecting the better initial dispersal; all fuels were within 4°. The differences reduced at 80 °C, 1.0 bar, where the LD injector had only 2° wider sprays. The angle increase with rising temperature was found to be 4–10° for the SE injector, while the LD injector only featured a small increase at 1.0 bar and up to 7° at 0.5 bar. At 80 °C, the differences between fuels became more obvious. Specifically, for 1.0 bar with the SE injector, gasoline and E25 (the fuels with the highest vapour pressures) clearly separated away from the rest of the fuels towards larger angles, indicating the onset of flash boiling. For the LD injector though, the differences amongst fuels remained generally quite small. The effect of temperature increase on E25 and gasoline manifested itself on the near-nozzle angle only for the first 1–2° CA after spray appearance; after that the angle fell back to the levels of all the other fuels. At 80 °C fuel temperature, reducing the gas pressure to 0.5 bar, resulted in larger angles for all fuels, except butanol, with both injectors. E25 and gasoline were still affected the strongest and had angles of 80° for the SE and 82° with the LD injector. The butanol mixtures followed with angles of 76° and 78° for the SE and LD, respectively. All mixtures were closer to gasoline than their respective base alcohol. Ethanol, subject to strong superheat, showed an angle increase from 74° to 76°. At nozzle closure (14° CA ASOI) the angle reduced faster for the hot fuels at 0.5 bar. Standard deviations were very low, about 1.5–2.5°.

5.2.3 Developed spray angle (0–25 mm)

The spray angle measured at 25 mm downstream of the nozzle exit is shown in **Figure 14**. The gasoline sprays of both injectors appeared at about the same time. This suggested that the initially earlier spray appearance at the nozzle tip of the LD injector was compensated for by the higher spray tip velocity of the SE. Exception to this was the 80 °C fuel sprays into 0.5 bar gas pressure where the LD sprays appeared about 1° CA earlier. The angle's development did not show a stable plateau but reached a peak value and successively reduced during injection for all cases except at 0.5 bar, 80 °C. Here, strong spray collapse led to a constant angle during injection. The LD injector showed larger angles than the SE, indicating again better spray dispersion. The difference between injectors was 4–5° at 20 °C and 1–4° at 80 °C. For the alcohol fuels at 20 °C, 1.0 bar, the angle was 42–47° for the SE injector and typically 48–52° for the LD injector. Butanol exhibited the smallest angle during the early stages of injection, just below that of ethanol. Again, most prominent difference between the two injectors was that fuels with high viscosity arrived significantly later at the point of measurement for the SE injector, where an almost stable angle was found with ongoing injection duration. All fuels appeared almost simultaneously with the LD injector, with only butanol trailing slightly. A much 'curvier' shape can be seen, with a larger peak value. This can be related to a recirculation structure breaking away from the spray tip (more dominant for the LD). At 80 °C, 1.0 bar, gasoline featured a significantly smaller spray angle than all other fuels with the SE nozzle. E25, despite having fully collapsed already, still showed more droplets detached from the spray core in the images and wider angles were quantified. The LD injector showed collapse and merging of individual spray plumes for all alcohol blends in the images and featured stronger recirculation patterns on the periphery of the sprays than gasoline. Gasoline collapsed the most with the SE injector, so that the shapes of the lines were similar between both injectors despite their different visual appearance. At 80 °C, 0.5 bar, all sprays except butanol had finally merged into a single spray structure and gasoline had the lowest angle, ~35° for both injectors. Some recirculation was still visible, more so for the LD injector. The alcohol mixtures had wider angles than gasoline with both injectors by about 2–3°; E25 appeared more collapsed than B16 and B25. The LD injector spray angles were ~2° above those of the SE. Ethanol's collapse was not as pronounced as that of the blends and the resulting angles were between 40–42°, slightly larger for the LD injector. Butanol still maintained its individual plumes

with the SE injector, showing a gradual angle reduction from 47° to 40° with ongoing injection. However, with the LD nozzle, butanol's plumes exhibited a degree of merging and the stronger separation of droplets from the spray centre resulted in larger angles (47° *vs.* 45°). Generally, fuels with largest near-nozzle 0–5 mm angles due to flash boiling resulted in strongest spray merging and collapse at 25 mm past the nozzle. The wider spray angles found for the LD injector, and the smaller delay, further supported previous observations of better spray dispersion and reduced susceptibility of the spray's geometry to fuel properties for this nozzle. The standard deviation of the 0–25 mm angle was similar for both injectors and mainly dependent on ambient pressure. It was lowest at 0.5 bar with values in the region of 1.0–1.5°, whilst at 1.0 bar it increased to levels of 1–4° with the lowest values recorded for ethanol and butanol.

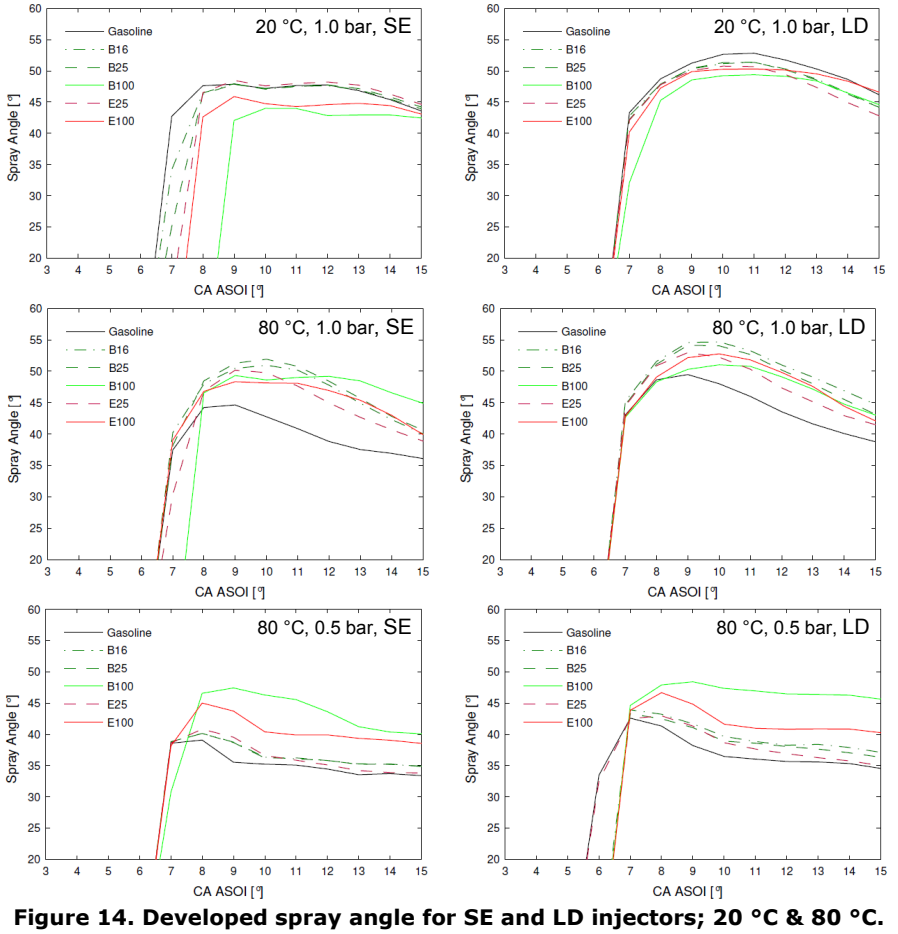

Figure 14. Developed spray angle for SE and LD injectors; 20 °C & 80 °C.

5.3 Droplet sizing

5.3.1 SMD of gasoline

The gasoline droplets arriving first at the PDA probe volume were largest in size, with SMD up to 30 µm at 20 °C and up to 18 µm at 80 °C. Large droplets were also found at the most outwards spray locations, but these were low in numbers. At late timings, past 2.8 ms ASOI, the droplets at the former spray centre region showed a small size increase (more so for 20 °C), possibly due to coalescence or to

differences in needle closure effects. It is noted that the higher flow rate of the LD injector did not seem to affect the time-averaged values of SMD much; this was verified by analysis of the SMD at individual times ASOI with both injectors but not presented here for brevity. **Figure 15** shows the SMD profile across the gasoline sprays (averaged in time) with both injectors. At 1.0 bar gas pressure, 20 °C fuel temperature, the SMD was 16–18 μm with both injectors. The large droplets at the spray border were more prominent at 1.0 bar than at 0.5 bar. At 80 °C, the droplets reduced to levels of 12–14 μm; the data also featured a larger plume width. The droplet velocities during nozzle opening peaked at about 80 m/s for 0.5 bar gas pressure and were a bit higher at 20 °C than at 80 °C. At 1.0 bar, the axial velocities reduced to 50 m/s in the spray core for both fuel temperatures and were larger by ~10% for the LD injector. The horizontal velocities were 15–20 m/s, higher at 0.5 bar and slightly larger for the LD. Overall, the droplet velocities followed similar trends to those described earlier for the penetration velocities.

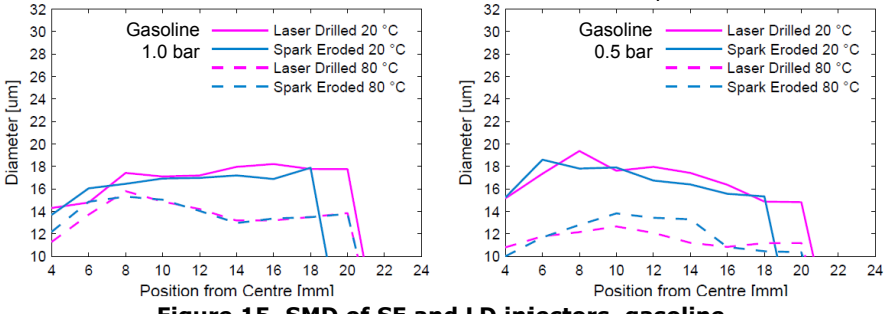

Figure 15. SMD of SE and LD injectors, gasoline.

The most obvious difference between the two injectors was the wider plume of the LD at 20 °C, in agreement with spray images. The LD also showed a marginally smaller SMD than the SE at 0.5 bar with both fuel temperatures. Small differences were also observed between the injectors at 1.0 bar, with the LD exhibiting sub-micron smaller droplets at 80 °C but larger ones at 20 °C. The somewhat larger SMD at 80 °C, 0.5 bar during the developed spray compensated for the smaller tip droplets and smaller floating droplets past nozzle closure. The wider plume of the LD injector at 20 °C was again witness to better fuel dispersion; yet the results featured larger droplet sizes (but only by 1–3%). At 80 °C, 0.5 bar the LD injector showed slightly reduced SMD profile. This could be due to denser spray of the SE injector at this condition, resulting in droplet coalescence or measurement bias towards few larger values. The SMD on its own requires great care when making comparisons as it is known for its ambiguity; two sprays can have same SMD but very different droplet distributions. The droplet histograms of both injectors are shown in **Figure 16**. These are closely mirroring each other. The 1.0 bar graph shows a peak around 8 μm for both temperatures. The 0.5 bar graph shows a narrower distribution with generally smaller droplets and a peak at ~6 μm.

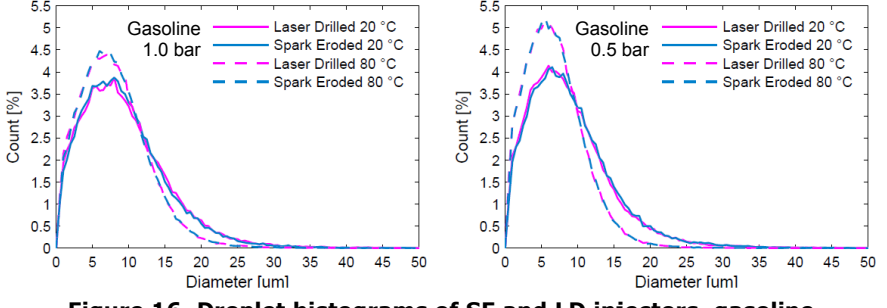

Figure 16. Droplet histograms of SE and LD injectors, gasoline.

The 20 °C sprays exhibited a distribution skewed to the right. The distribution at 80 °C was narrower and lacked droplets exceeding 22 μm. At 20 °C, droplets up to 30 μm were clearly present in the histograms and resulted in larger overall SMD. It needs to be noted though that, as initially observed by imaging, the clustered droplets at the spray tip had indeed different sizes. The LD showed about 8–10% smaller SMD over the first 1 ms ASOI than the SE at most conditions.

5.3.2 SMD of alcohol fuels

The SMD averaged over all locations and time is shown in **Figure 17** for 1.0 bar and **Figure 18** for 0.5 bar. The standard deviations have also been included as error bars. The LD showed lower sensitivity to fuel type in terms of spray geometry but it returned clearly larger SMD for the pure alcohols. Ethanol's SMD at 20 °C was higher with the LD by 10% at 1.0 bar and 5% at 0.5 bar. The difference was reduced at 80 °C, with 4% larger SMD at 1.0 bar and very similar at 0.5 bar. For butanol at 20 °C, the LD returned larger SMD by ~12%. At 80 °C, the SMD of the LD was greater by 10% at 1.0 bar and 8% at 0.5 bar. The 0.5 bar reduction had little effect on the SMD at 20 °C for both injectors. Strong SMD reduction was found at 80 °C for gasoline (16–20%); smaller for ethanol (6–11%) and butanol (3–5%).

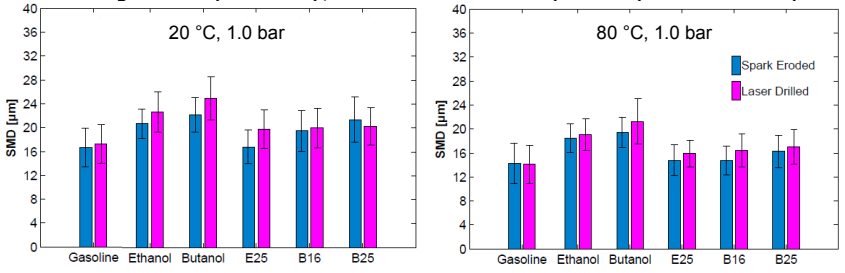

Figure 17. SMD of SE and LD injectors, all fuels; 1.0 bar, 20 °C & 80 °C.

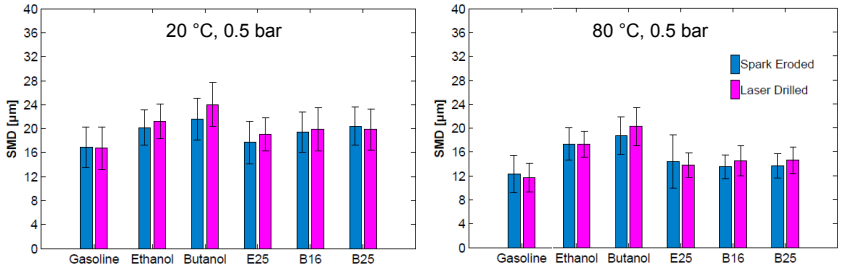

Figure 18. SMD of SE and LD injectors, all fuels; 0.5 bar, 20 °C & 80 °C.

Ethanol's and butanol's droplet histograms are given in **Figures 19–20**. These underline the poorer overall atomisation of the LD injector by the strongly skewed shape towards larger droplets and the lower count of droplets around 8–10 μm. However, when the SMD was calculated over the early injection event, this was found to be 5–10% smaller for the LD and agreed well with the smaller droplet clusters observed at the tip of the spray in the images. E25 featured an increase in SMD of up to 2 μm when compared to gasoline. Interestingly, 1.0 bar showed smaller differences than the 0.5 bar case. E25's SMD at 80 °C was typically reduced by 2–4 μm compared to 20 °C. At 0.5 bar, 80 °C, E25 was strongly flash boiling and measurements in the spray's centre were found to return lower data counts and generally larger values than on the periphery, along with higher standard deviations. Droplet coalescence in the dense spray core may have biased the result towards larger SMD. Especially in the late stages of injection, the SMD bins contained some large droplets (of the order 25 μm) which would contribute

significantly to larger overall SMD. Such large droplets were not present when data were taken at 80 bar injection pressure and it is possible that these were created by after-injection effects related to needle closing; some late needle bouncing that led to secondary injection was observed for the LD nozzle by high-speed imaging.

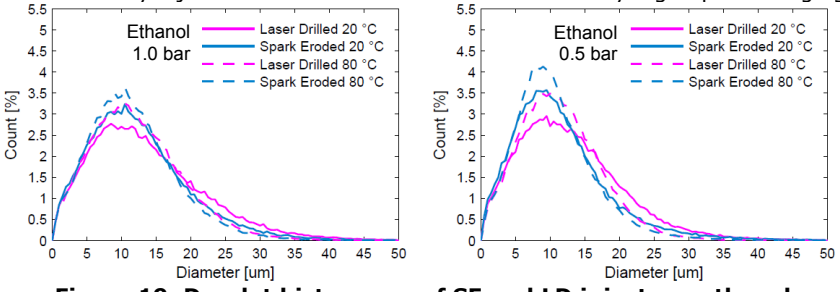

Figure 19. Droplet histograms of SE and LD injectors, ethanol.

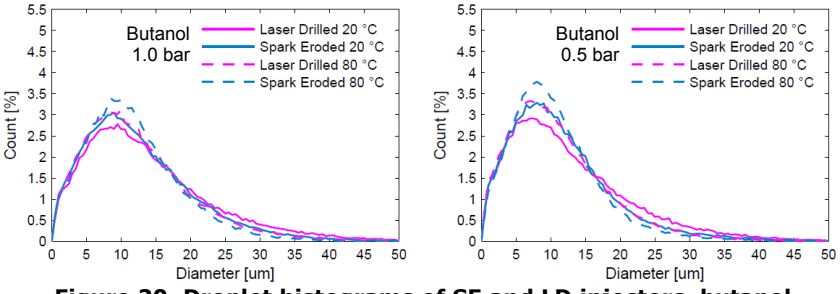

Figure 20. Droplet histograms of SE and LD injectors, butanol.

E25 showed larger SMD than gasoline with the LD injector (by 1–2 μm), but lower than ethanol at all conditions. E25's droplet sizes were generally 4–7% higher than what one would obtain by linear interpolation between the sizes obtained for the base components (with higher temperatures being closer to linearity). Droplets from the LD injector were typically larger by 7–17% than from the SE, with the exception of the 0.5 bar gas pressure, 80 °C fuel temperature, where the strongly flashing E25 fuel had 4% smaller droplets with the LD injector. Considering that E25's vapour pressure was larger than gasoline's, it may be said that even though the vapour pressure is of importance for phase change due to cavitation and flash boiling effects, there must be an overriding mechanism that compensates for this, such as a combination of viscosity and latent heat effects. The E25 droplet histogram of the LD injector showed that 20 °C resulted in wide distribution and strongly skewed shape towards larger droplets. Hot fuel conditions also showed a smaller percentage of small droplets for the LD injector than for the SE. However, the large amount of droplets above 20 μm was much smaller than at 20 °C. In general, the data showed that the LD injector performed significantly worse with ethanol and E25 in terms of droplet sizes. B16 and B25 showed much larger SMD than gasoline at 20 °C with the SE injector at both gas pressures. Specifically, SMD values of ~19.5 μm were recorded for B16 and ~20–21.5 μm for B25. Particularly for B25, the SMD was significantly closer to that of butanol (~22 μm) than that of gasoline (<17 μm). Increasing the fuel temperature to 80 °C at 1.0 bar gas pressure brought the mixtures' SMD much closer to gasoline's SMD; B16 recorded 15 μm, B25 16 μm, whilst gasoline's SMD was 14 μm. At 0.5 bar both mixtures behaved similarly and exhibited SMD of ~13.5 μm, just about 1 μm larger than gasoline's. It was generally found that decreasing the pressure led to slightly smaller droplets; much stronger reduction followed with temperature increase. The LD injector showed smaller differences between B16 and B25. Their SMD was ~3 μm larger than gasoline's and 4–6 μm smaller than butanol's. Similarly to butanol,

B16 and B25 generally also showed larger droplets with the LD injector. The exception was B25 at 20 °C which exhibited 2–5% smaller SMD; this was due to fewer large droplets with diameters beyond 25 μm and 18 μm for 1.0 bar and 0.5 bar gas pressure, respectively. The droplet histograms of B16 and B25 held no surprise as their trends were quite akin to those of the other alcohol fuels. The LD injector showed a slightly stronger bias towards larger droplets (especially at 1.0 bar) and the percentage of small droplets was generally lower, more so at 80 °C than at 20 °C. At 80 °C the droplets exhibited a peak at ~1 μm smaller diameter than at 20 °C and showed a narrower distribution. Droplets exceeding 25–30 μm at 80 °C were rare, while at 20 °C a large number of droplets existed up to 35–40 μm.

6. SUMMARY AND CONCLUSIONS

The current investigation quantified the differences in spray geometry and droplet sizes for two multi-hole injectors which were declared 'like-for-like' replacements. The original nozzle was manufactured by spark erosion and the replacement by Laser drilling. Gasoline, ethanol, butanol, E25, B25 and B16 fuels were employed. Testing involved 20 °C, 80 °C injector temperature and 0.5 bar, 1.0 bar gas pressure. Fuel pressure was 120 bar. Conclusions can be summarised as follows:

- Microscopy showed that the nozzle-hole geometries of the two injectors were different, with the SE featuring a two-step inner-outer cylindrical bore and the LD featuring an expanding conical inner hole and a cylindrical outer hole.
- Flow tests showed ~10% higher flow rate for the LD injector, also indicating potential differences in two-phase flow patterns inside the nozzles.
- The spray images and PDA data indicated wider sprays for the LD injector.
- Spray shapes differed amongst fuels, more so at 80 °C where gasoline sprays collapsed more than ethanol's whilst no clear collapse occurred for butanol.
- The alcohols showed a delay in appearing at the nozzle with both injectors. Appearance was earlier for the LD injector, especially at 20 °C.
- The gasoline-alcohol blends were similar to gasoline in terms of spray shape but didn't collapse as strongly at 80 °C. Flash boiling was distinctly stronger with ethanol than butanol blends. E25 was closer to gasoline than B16 or B25.
- Differences in spray geometry between fuels were smaller with the LD injector than with the SE, as demonstrated by spray penetration and angle data.
- Flash boiling fuels featured a strong near-nozzle spray angle increase (0–5 mm past the nozzle) while subsequent spray collapse returned reduced downstream angles (0–25 mm past the nozzle) for both injectors.
- Butanol's spray angles were largely insensitive to conditions for both injectors.
- The LD injector, despite its higher flow rate and faster early penetration, achieved smaller axial penetration than the SE past 8° CA ASOI for most conditions. This was associated with its wider radial dispersion.
- At 0.5 bar, 80 °C fuel temperature, the LD showed greater spray collapse and longer axial penetration. This can work in favour of the SE in terms of piston impingement and emissions. However, there is margin for improvement for the LD since its higher flow rate would require shorter injection.
- Gasoline sprays showed similar droplet size histograms with both injectors. The LD exhibited marginally smaller SMD than the SE at 0.5 bar with both 20 °C and 80 °C. Marginal differences were also observed at 1.0 bar, with the LD exhibiting sub 1 μm smaller droplets at 80 °C but larger at 20 °C.
- The LD had larger ethanol and butanol SMD than the SE. The histograms were clearly skewed towards larger droplets with reduced count of small droplets.
- The SMD of E25 was close to gasoline's with the SE but much larger with the LD. The difference reduced close to boiling and inverted at 80 °C, 0.5 bar.
- B25 returned slightly smaller droplets with the LD injector at 20 °C, 0.5 bar, but this reversed at 80 °C. B16's SMD was always larger with the LD. B16 had smaller droplets than B25 with the SE, but almost the same with the LD.

- However, the LD injector exhibited smaller clustered droplets at the initial tip of the spray for all fuel types. This was observed by imaging and then quantified by droplet sizing to be about 5–10%, depending on conditions.
- Even though the spray appeared much better dispersed for the LD injector than the SE, the overall SMD of the LD was typically larger, showing that better dispersion does not necessarily also mean better overall atomisation.

REFERENCE LIST

1. Whitaker, P., Kapus, P., Ogris, M. and Hollerer, P., "Measures to Reduce Particulate Emissions from Gasoline DI Engines", SAE 2011-01-1219, 2011.
2. Yaws, C.L., "Yaws' Handbook of Thermodynamic and Physical Properties of Chemical Compounds", Knovel, 2003.
3. Chen, L. and Stone, R., "Measurement of Enthalpies of Vaporization of *iso*-Octane and Ethanol Blends and Their Effects on PM Emissions from a GDI Engine", Energy & Fuels, 25:1254–1259, 2011.
4. Andersen, V.F., Anderson, J.E., Wallington, T.J., Mueller, S.A. and Nielsen, O.J., "Distillation Curves for Alcohol-Gasoline Blends", Energy & Fuels, 24:2683–2691, 2010.
5. Andersen, V.F., Anderson, J.E., Wallington, T.J., Mueller, S.A. and Nielsen, O.J., "Vapor Pressures of Alcohol-Gasoline Blends", Energy & Fuels, 24:3647–3654, 2010.
6. Hull, A., Golubkov, I., Kronberg, B., Marandzheva, T. and Stam, J. van, "An Alternative Fuel for SI Engines", Int. J. Eng. Res., 7:203–214, 2006.
7. Ferrando, N., Defoille, D., Lachet, V. and Boutin, A., "Ethanol Gasoline Bubble Pressure Determination: Experimental and Monte Carlo Modeling", Fluid Phase Equilibria, 299:132–140, 2010.
8. Macián, V., Bermudez, V., Payri, R. and Gimeno, J., "New Technique for Determination of Internal Geometry of a Diesel Nozzle with the Use of Silicone Methodology", Experimental Techniques, 27:39–43, 2003.
9. Hung, D.L.S., Harrington, D.L., Gandi, A.H., Markle, L.E., Parrish, S.E., Shakal, J.S., Sayar, H.C., Steven, D. and Kramer, J.L., "Gasoline Fuel Injector Spray Measurement and Characterization – A New SAE J2715 Recommended Practice", SAE Paper 2008-01-1068, 2008.
10. van Romunde, Z.R., Aleiferis, P.G., Cracknell, R.F. and Walmsley, H.L., "Effect of Fuel Properties on Spray Development from a Multi-Hole DISI Engine Injector", SAE Transactions, J. of Engines, 116:1313–1331, 2007.
11. Serras-Pereira, J., Aleiferis, P.G, Richardson, D. and Wallace, S., "Characteristics of Ethanol, Butanol, *iso*-Octane and Gasoline Sprays and Combustion from a Multi-Hole Injector in a DISI Engine", SAE J. of Fuels & Lubs, 1:893–909, 2008.
12. Aleiferis, P.G., Serras-Pereira, J., van Romunde, Z.R., Caine, J. and Wirth, M., "Mechanisms of Spray Formation and Combustion from a Multi-Hole Injector with E85 and Gasoline", Comb. & Flame, 157:735–756, 2010.
13. Aleiferis, P.G. and van Romunde, Z.R., "An Analysis of Spray Development with *iso*-Octane, *n*-Pentane, Gasoline, Ethanol and *n*-Butanol from a Multi-Hole Injector under Hot Fuel Conditions", Fuel, 105:143–168, 2013.
14. Albrecht, H.-E., Damaschke, N., Borys, M. and Tropea, C., "Laser Doppler and Phase Doppler Measurement Techniques", Springer, 2002.
15. Pitcher, G., Wigley G. and Saffman. M., "Velocity and Drop Size Measurements in Fuel Sprays in a DI Diesel Engine", Part. & Part. Syst. Char., 7:160–168, 1990.
16. Pitcher G., Wigley G. and Saffman M., "Sensitivity of Dropsize Measurements by Phase Doppler Anemometry to Refractive Index Changes in Combusting Fuel Sprays", Applications of Laser Techniques to Fluid Mechanics, pp. 227–247, Springer-Verlag, 1991.
17. Serras-Pereira, J., Aleiferis, P.G., Walmsley, H.L., Davies, T.J. and Cracknell, R.F., "Heat Flux Characteristics of Spray Wall Impingement with Ethanol, Butanol, *iso*-Octane, Gasoline and E10 Fuels", Int. J. Heat & Fluid Flow, 44:662–683, 2013.